Significance of the singularities for ion channeling through nanostructured materials

M. Ćosić

Laboratory of Physics, Vinča Institute of Nuclear Sciences, University of Belgrade,
P. O. Box 522, 11001 Belgrade, Serbia

10th of January 2023.

Table of content

Channels in crystals

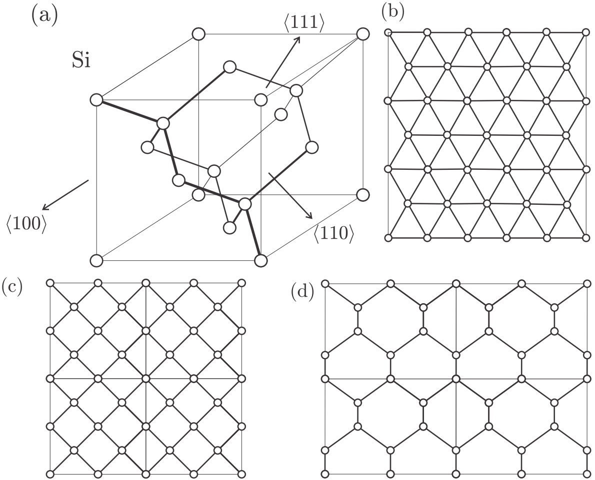

Figure 1: (a) The unit cell of the *Si* crystal. Projection of the crystal lattice on: (b) [111], (c) [100], and (d) [110] planes, respectively.

Channels in carbon nanotubes

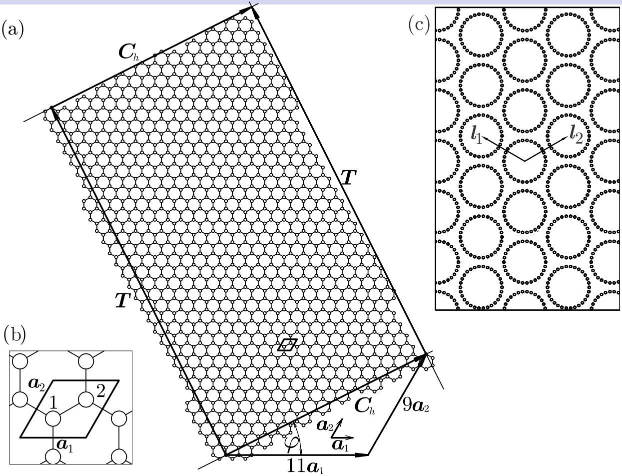

Figure 2: (a) Unit cell of the chiral single-walled carbon nanotube $C_h = (11, 9)$; (b) Unit cell of the graphite plane. (c) The normal cross-section through the bundle of single-walled carbon nanotube.

Channeling effect

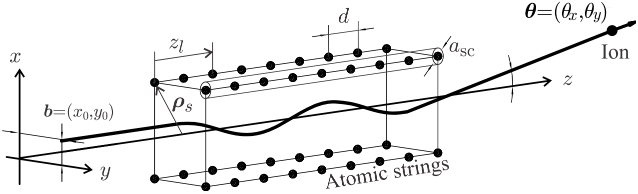

Figure 3: Schematic of the ion channeling process.

Positions of atoms:

$$\boldsymbol{r}_{sl} = \boldsymbol{\rho}_s + z_l \boldsymbol{e}_z, \quad s = 1, 2, \ldots, N, \quad l = 1, 2, \ldots, M.$$

Potential energies of ion-solid interaction:

$$U(\boldsymbol{r}) = \sum_{sl} V_{sl} = \sum_{sl} V(\boldsymbol{r} - \boldsymbol{r}_{sl}), \quad V(\boldsymbol{\rho}) = \frac{Z_1 Z_2 e^2}{4\pi\varepsilon_0 \|\boldsymbol{\rho}\|} \Phi_{\mathrm{sc}} \left(\frac{\|\boldsymbol{\rho}\|}{a_{\mathrm{sc}}} \right).$$

Continuum approximation:

$$U(\boldsymbol{r}) \approx \sum_s U_s(\boldsymbol{\rho}) = \sum_s \frac{1}{d} \int_z V(\boldsymbol{r} - \boldsymbol{\rho}_s) dz, \quad \Theta_c = \sqrt{\frac{U(\boldsymbol{\rho}_s + a_{\mathrm{sc}} \boldsymbol{e}_z)}{E}}$$

Model of crystal rainbow

For high energies channeling is considered as a single small angle scattering event on the crystal potential.
Momentum approximation

$$\boldsymbol{\theta}(\boldsymbol{b}) = -\frac{1}{2E}\sum_{s=1}^{M}\sum_{l=1}^{N}\int_z \nabla V_{sl}(\boldsymbol{b}) = -\frac{L}{2E}\nabla\sum_{s=1}^{M}U_s(\boldsymbol{b})$$

defines a mapping $\boldsymbol{b} \to \boldsymbol{\theta}$. Differential cross-section

$$\sigma_{\mathrm{diff}} = \frac{1}{|J|}, \quad J(\boldsymbol{b}) = \frac{\partial\theta_x}{\partial x_0}\frac{\partial\theta_y}{\partial y_0} - \frac{\partial\theta_x}{\partial y_0}\frac{\partial\theta_y}{\partial x_0}$$

Rainbow lines in the impact parameter (IP) plane are solutions of the equation

$$J(\boldsymbol{b}) = 0.$$

Their image in the scattered angle (SA) plane are called angular rainbow lines.

Model of crystal rainbow

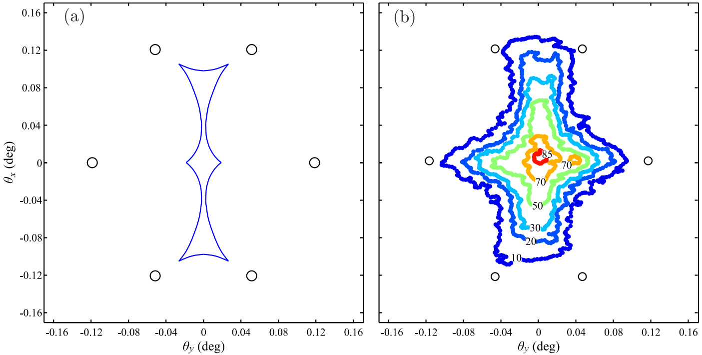

Figure 4: (a) Rainbow line in the TA plane for 7-MeV protons transmitted through ⟨110⟩ channel of 150-nm long Si crystal, assuming Lindhard's potential. (b) Corresponding experimental angular distribution. Open circles correspond to angular coordinates of atomic strings.

Elements of catastrophe theory

Let

$$F(x_1, \ldots, x_m; c_1, \ldots, c_n),$$

be a function family depending on state variables $x_1, \ldots, x_m$ and parameters $c_1, \ldots, c_n$.
On variations of parameters, family F changes the number and type of its critical points in the vicinity of which it is equivalent to the certain polynomial prototype

$$G(\chi_1, \ldots, \chi_r; \alpha_1, \ldots, \alpha_s),$$

depending on new state variables $\chi_1, \ldots, \chi_r$ and parameters $\alpha_1, \ldots, \alpha_s$ such that $r \leq m$, $s \leq n$ and there are equivalences between

$$\nabla_x F = 0 \Leftrightarrow \nabla_\chi G = 0, \text{ critical points and}$$
$$\boldsymbol{H}_x F = 0 \Leftrightarrow \boldsymbol{H}_\chi G = 0, \text{ degenerate critical points.}$$

Crystal rainbows as catastrophic effect

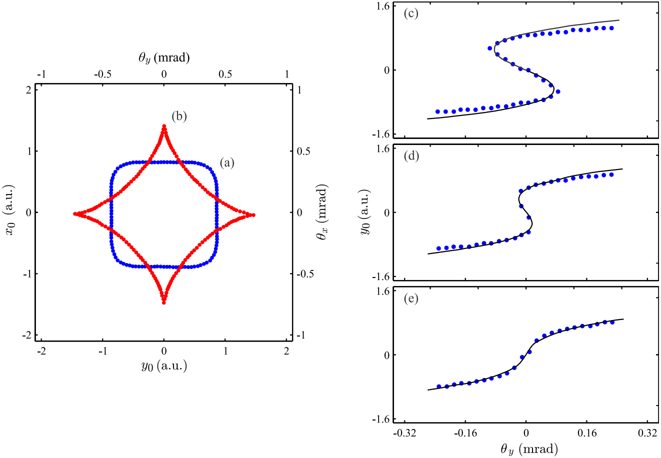

Figure 5: Rainbow lines in (a) the IP, and (b) SA plane for 10-MeV protons transmitted through 100-nm long ⟨100⟩ channels of Au crystal. (c-e) The unfolding of the function $y(\theta_x, \theta_y)$ for: θ_x=0.51, 0.65 and 0.79 mrad. Dots represent results of numerical simulation, lines fit by cusp catastrophe.

Theory of rainbows in crystals and nanotubes

Solution of the equation of motion

$$m\frac{d^2\boldsymbol{\rho}}{dt^2} = -\nabla U(\boldsymbol{\rho}),$$

define two maps

$$x = x(\boldsymbol{b}), \qquad \theta_x = \theta_x(\boldsymbol{b});$$
$$y = y(\boldsymbol{b}), \qquad \theta_y = \theta_y(\boldsymbol{b}).$$

where $\theta_x \approx v_x/v_z$ and $\theta_y \approx v_y/v_z$.

$$\sigma^r_{\mathrm{diff}} = \frac{1}{|J_r|}, \qquad J_r = \frac{\partial x}{\partial x_0}\frac{\partial y}{\partial y_0} - \frac{\partial x}{\partial y_0}\frac{\partial y}{\partial x_0};$$
$$\sigma^\theta_{\mathrm{diff}} = \frac{1}{|J_\theta|}, \qquad J_\theta = \frac{\partial \theta_x}{\partial x_0}\frac{\partial \theta_y}{\partial y_0} - \frac{\partial \theta_x}{\partial y_0}\frac{\partial \theta_y}{\partial x_0}.$$

Rainbow lines in IP plane are solutions of equations $J_r = 0$, $J_\theta = 0$. Their images in the TP or SA planes are spatial and angular rainbows, respectively.

Evolution of crystal rainbows

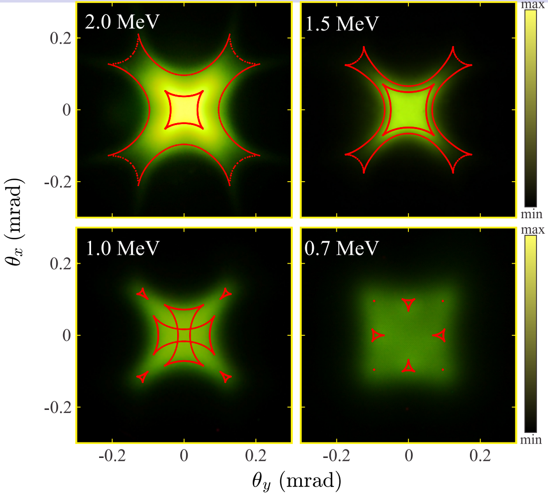

Figure 6: Experimental angular distribution of 2.0, 1.5, 1.0, and 0.7-MeV protons transmitted through 55-nm long ⟨100⟩ channel of Si crystal and the corresponding rainbow lines in SA plane (red lines).

Quantum rainbow channeling in nanotubes

Evolution of the positron wave function in the spatial representation $\psi_s(\boldsymbol{\rho}, t; \boldsymbol{b})$ is obtained from solution of the Schrödinger equation

$$i\hbar \frac{\partial}{\partial t} \psi_s(\boldsymbol{\rho}, t; \boldsymbol{b}) = \left[-\frac{\hbar^2}{2m} \nabla^2 + U(\boldsymbol{\rho}) \right] \psi_s(\boldsymbol{\rho}, t; \boldsymbol{b}).$$

Evolution of wave function in the angular representation $\psi_a(\boldsymbol{\theta}, t; \boldsymbol{b})$ is obtained from ψ_s via Fourier transformation.
For $t = 0$, both ψ_s and ψ_a are represented by Gaussian wave packed having standard deviations σ_r and σ_θ, respectively.
Spatial and angular distributions of positron beam Y_r and Y_a, respectively, are:

$$Y_r(\boldsymbol{\rho}, t) = \sum_{\boldsymbol{b}} c_{\boldsymbol{b}} |\psi_r(\boldsymbol{\rho}, t; \boldsymbol{b})|^2, \quad Y_\theta(\boldsymbol{\theta}, t) = \sum_{\boldsymbol{b}} c_{\boldsymbol{b}} |\psi_a(\boldsymbol{\theta}, t; \boldsymbol{b})|^2,$$

parameters $c_{\boldsymbol{b}}$ were chosen in such a manner that initially Y_r is uniform, while Y_a is Gaussian distribution having FWHM Δ_θ.

Wave-packet dynamics

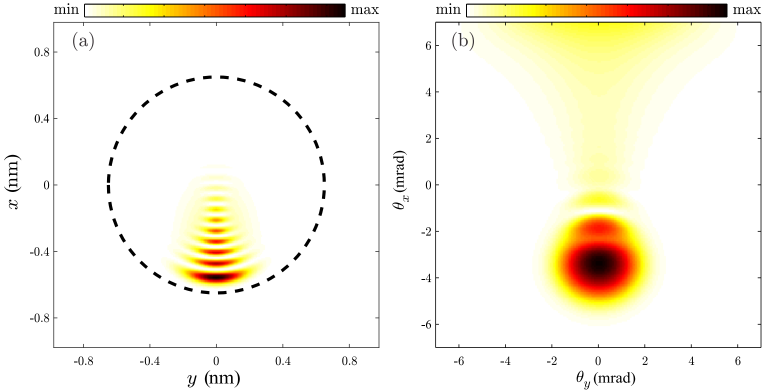

Figure 7: The wave-packet of impact parameter $\boldsymbol{b} = (0.624, 0)$ nm at the exit of 200 nm long chiral SWCNT (14,4) in (a) spatial, and (b) angular representation, respectively.

Young's explanation of the rainbow effect

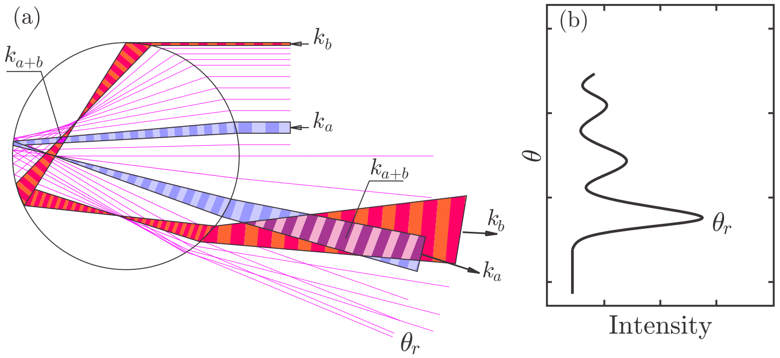

Figure 8: (a) Schematics of the interference of the wave-trains traveling along geometrical rays. The strongest light intensity modulation happens when wave crests and troughs meet. (b) The light intensity in the vicinity of the rainbow angle θ_r.

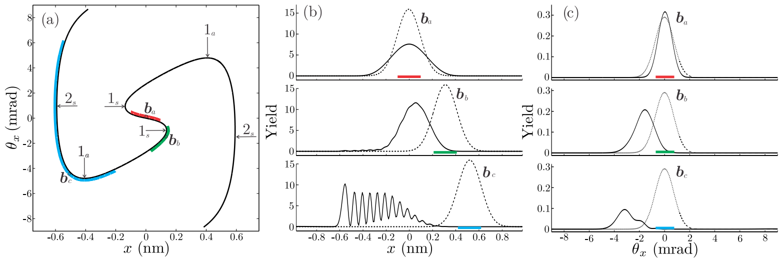

Figure 9: (a) The rainbow diagram for 1MeV positron transmitted through a 200 nm long (14, 4) SWCNT. The initial and final probability distributions in (b) spatial and (c) angular representation.

Semiclassical theory of the rainbow channeling

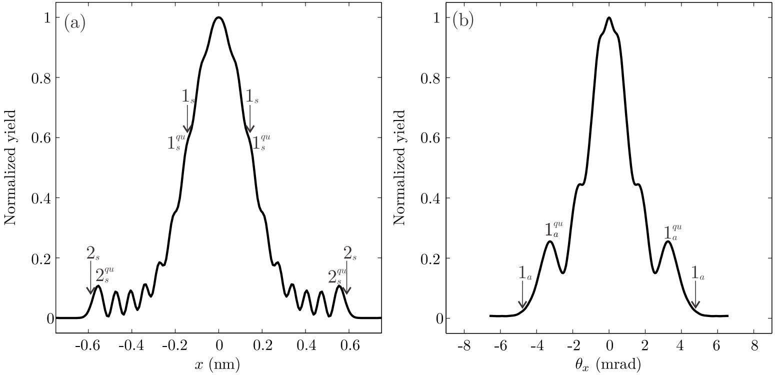

Figure 10: (a) Spatial and (b) angular distributions of 1MeV Gaussian positron beam, having SD $\Delta = 0.1\Theta_c$ transmitted through 200nm long $(14, 4)$ SWCNT.

The positron transmission through nanotube (11,9)

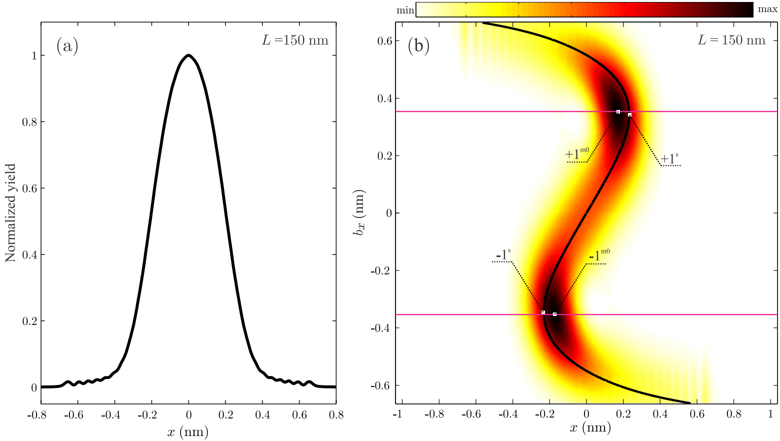

Figure 11: (a) The slice through probability density of 1-MeV positron beam. (b) Corresponding slices through individual wave packets.

Families of Amplitude Squared and Phase Functions

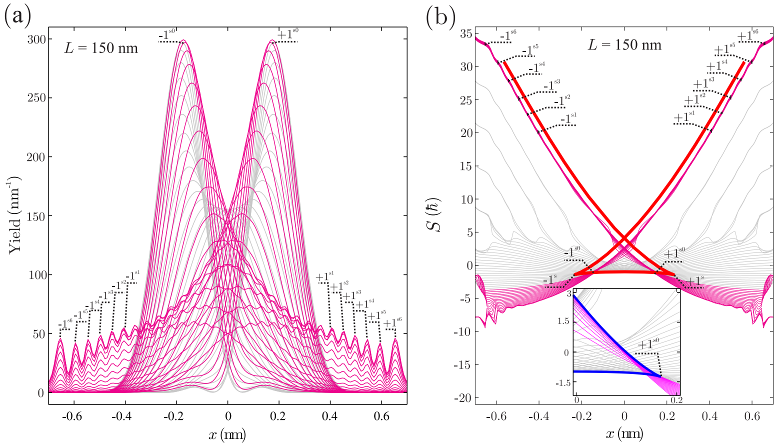

Figure 12: (a) The family of wave-packet probability density functions; (b) The corresponding family of wave-packet phase functions.

Superfocusing effect

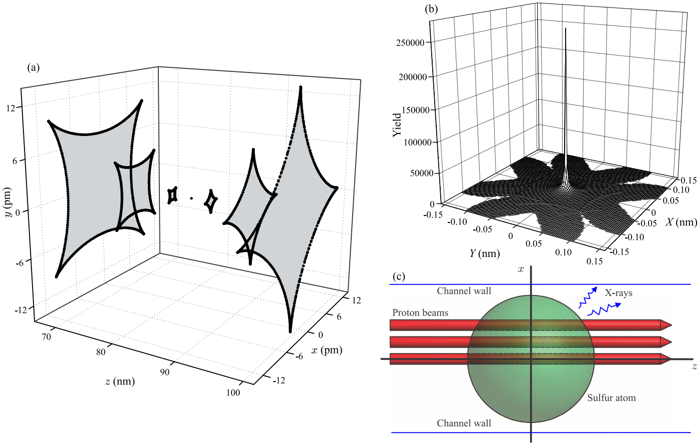

Figure 13: (a) Evolution of rainbow lines in the TP plane in the vicinity of the superfocus for 2-MeV protons in the ⟨100⟩ channel of Si. (b) Spatial distribution at the superfocus. (c) Illustration of the proton beam's interaction with the S atom's inner shells inserted in the Si crystal's channel.

Accurate proton-Si potential

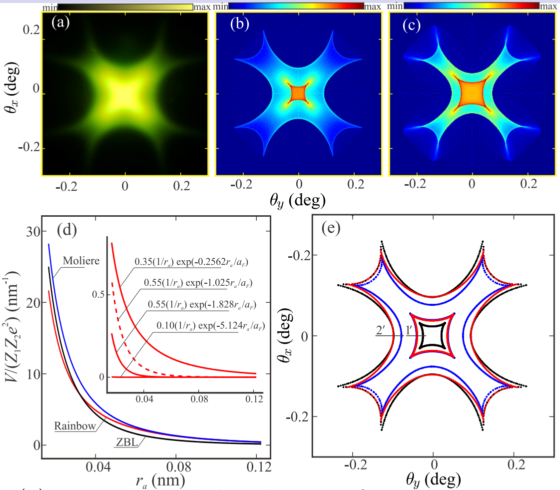

Figure 14: (a) Experimental distribution of 2-MeV protons transmitted through 55-nm long ⟨100⟩ Si channel. Theoretical distributions were obtained using: (b) ZBL and (c) Molière's potential. (d) Proton-Si potentials. (e) Rainbow lines in TA plane.

Characterization of SWCNT with defects

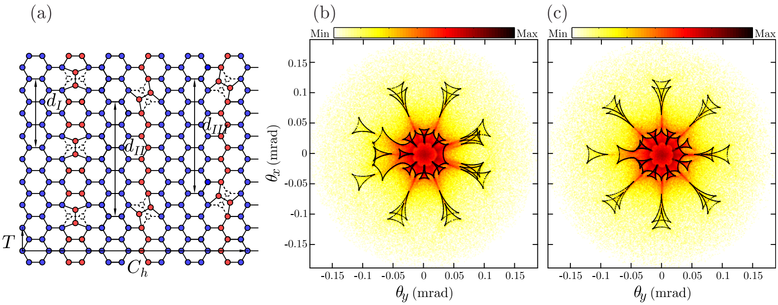

Figure 15: (a) The part of the unrolled sheet forming an armchair SWCNT with Stone–Wales defects. Atomic strings created or modified by the presence of defects are colored red. Angular yields of 1-GeV protons transmitted through a 200-nm long armchair SWCNT (4, 4), together with corresponding rainbow lines for defects of (b) type I and; (c) type II or III. Linear density of the defects in all cases was $l_{\text{def}} = 2.005$ nm^{-1}.

Conclusions

- Classical rainbow channeling is a complex emergent effect, i.e., irreducible to the sum of contributions of individual atomic strings.
- Classical rainbows are manifestations of folds of the equilibrium surface.
- Classical rainbows are related to the envelope of the trajectory family.
- Quantum rainbows are caused by wave packet coordinate self–interference and are linked to the singularities of the phase function family.